Comparison of ^{18}F-Labeled Fluoroalkylphosphonium Cations with ^{13}N-NH_3 for PET Myocardial Perfusion Imaging

Dong-Yeon Kim[1], Hyeon Sik Kim[1], Sybille Reder[2], Jin Hai Zheng[1], Michael Herz[2], Takahiro Higuchi[2], AYoung Pyo[1], Hee-Seung Bom[1], Markus Schwaiger[2], and Jung-Joon Min[1]

[1]*Department of Nuclear Medicine, Chonnam National University Hwasun Hospital, Hwasun, Korea; and* [2]*Department of Nuclear Medicine, Klinikum Rechts der Isar, Technische Universität München, Munich, Germany*

Despite substantial advances in the diagnosis of cardiovascular disease, there is a need for ^{18}F-labeled myocardial perfusion agents for the diagnosis of ischemic heart disease because current PET tracers for myocardial perfusion imaging have a short half-life that limits their widespread clinical use in PET. Thus, ^{18}F-labeled fluoroalkylphosphonium derivatives (^{18}F-FATPs), including (5-^{18}F-fluoropentyl)triphenylphosphonium cation (^{18}F-FPTP), (6-^{18}F-fluorohexyl)triphenylphosphonium cation (^{18}F-FHTP), and (2-(2-^{18}F-fluoroethoxy)ethyl)triphenylphosphonium cation (^{18}F-FETP), were synthesized. The myocardial extraction and image quality of the ^{18}F-FATPs were compared with those of ^{13}N-NH_3 in rat models. **Methods:** The first-pass extraction fraction (EF) values of the ^{18}F-FATPs (^{18}F-FPTP, ^{18}F-FHTP, ^{18}F-FETP) and ^{13}N-NH_3 were measured in isolated rat hearts perfused with the Langendorff method (flow velocities, 0.5, 4.0, 8.0, and 16.0 mL/min). Normal and myocardial infarction rats were imaged with small-animal PET after intravenous injection of 37 MBq of ^{18}F-FATPs and ^{13}N-NH_3. To determine pharmacokinetics, a region of interest was drawn around the heart, and time–activity curves of the ^{18}F-FATPs and ^{13}N-NH_3 were generated to obtain the counts per pixel per second. Defect size was analyzed on the basis of polar map images of ^{18}F-FATPs and ^{13}N-NH_3. **Results:** The EF values of ^{18}F-FATPs and ^{13}N-NH_3 were comparable at low flow velocity (0.5 mL/min), whereas at higher flows EF values of ^{18}F-FATPs were significantly higher than those of ^{13}N-NH_3 (4.0, 8.0, and 16.0 mL/min, $P < 0.05$). Myocardium-to-liver ratios of ^{18}F-FPTP, ^{18}F-FHTP, ^{18}F-FETP, and ^{13}N-NH_3 were 2.10 ± 0.30, 4.36 ± 0.20, 3.88 ± 1.03, and 0.70 ± 0.09, respectively, 10 min after injection, whereas myocardium-to-lung ratios were 5.00 ± 0.25, 4.33 ± 0.20, 7.98 ± 1.23, and 2.26 ± 0.14, respectively. Although ^{18}F-FATPs and ^{13}N-NH_3 sharply delineated myocardial perfusion defects, defect size on the ^{13}N-NH_3 images was significantly smaller than on the ^{18}F-FATP images soon after tracer injection (0–10 min, $P = 0.027$). **Conclusion:** ^{18}F-FATPs exhibit higher EF values and more rapid clearance from the liver and lung than ^{13}N-NH_3 in normal rats, which led to excellent image quality in a rat model of coronary occlusion. Therefore, ^{18}F-FATPs are promising new PET radiopharmaceuticals for myocardial perfusion imaging.

Key Words: ^{18}F-fluoroalkylphosphonium cations; perfusion; first-pass extraction fraction; cardiac PET; myocardial infarction

J Nucl Med 2015; 56:1581–1586
DOI: 10.2967/jnumed.115.156794

Since the 1980s, SPECT has been the most widely applied method to assess myocardial blood flow and diagnose coronary artery disease (*1*). Notably, ^{99m}Tc-sestamibi, ^{99m}Tc-tetrofosmin, and ^{201}Tl are attractive surrogates for myocardial perfusion imaging using SPECT (*2,3*). However, the technical limitations of SPECT imaging, such as the absence of a standardized method for correction of photon attenuation and significant uptake of SPECT tracers in organs adjacent to the heart, may compromise the delineation of small lesions and limit the diagnostic accuracy of SPECT (*4*). PET has several technical advantages over SPECT including higher spatial resolution and a standardized method for the correction of photon attenuation. PET imaging also enables quantitative measurements of myocardial blood flow because it allows accurate determinations of rapidly changing tissue counts over time. Because of these advantages, it allows quantitative measures of myocardial tracer uptake and regional myocardial blood flow (*5*). However, the PET tracers currently used for myocardial perfusion imaging have a short half-life (^{13}N-NH_3, 9.97 min; ^{82}Rb, 1.27 min; ^{15}O-H_2O, 2.04 min), limiting widespread clinical use of PET because of the need for an on-site cyclotron or generator (*6,7*). The use of ^{18}F-labeled myocardial perfusion agents could overcome these limitations and simplify clinical protocols as a result of the longer half-life (109.8 min) and better spatial resolution and quantification (*5,8*).

To address this unmet clinical need, several publications have proposed ^{18}F-labeled phosphonium cations as myocardial imaging agents (*9–16*). Similar to SPECT tracers such as ^{99m}Tc-sestamibi and ^{99m}Tc-tetrofosmin, phosphonium cations accumulate in cardiomyocytes as a result of the higher mitochondrial membrane potential (*11,17–20*). Previously, we reported the synthesis and characterization of novel ^{18}F-labeled fluoroalkylphosphonium derivatives (^{18}F-FATPs), including (5-^{18}F-fluoropentyl)triphenylphosphonium cation (^{18}F-FPTP), (6-^{18}F-fluorohexyl)triphenylphosphonium cation (^{18}F-FHTP), and (2-(2-^{18}F-fluoroethoxy)ethyl)triphenylphosphonium cation (^{18}F-FETP), as a voltage sensor for myocardial imaging (*9,10,16*). In vivo biodistribution and imaging studies of ^{18}F-FATPs demonstrated intense initial myocardial uptake and retention of these tracers, with rapid clearance from liver and lung. Sharp delineation of areas of myocardial ischemia was achieved, suggesting the potential for use of these moieties as tracers of myocardial perfusion

Received Mar. 2, 2015; revision accepted May 29, 2015.
For correspondence or reprints contact either of the following:
Jung-Joon Min, Department of Nuclear Medicine, Chonnam National University Hwasun Hospital, 160 Ilsimri, Hwasun, Jeonnam 519-763, Republic of Korea.
E-mail: jjmin@jnu.ac.kr
Markus Schwaiger, Nuklearmedizinische, Klinik der Technischen Universität München, Ismaninger Strasse 22, 81675, Munich, Germany.
E-mail: markus.schwaiger@tum.de
Published online Jun. 11, 2015.

for clinical imaging. Therefore, further characterization of ^{18}F-FATPs to evaluate first-pass myocardial extraction and a comparison with the standard PET tracer ^{13}N-NH_3 are required. To determine whether ^{18}F-FATPs are comparable to ^{13}N-NH_3 as PET perfusion tracers and to provide better image quality than that currently provided by ^{13}N-NH_3 for the detection of myocardial infarction in rats, we compared first-pass extraction fraction (EF) values and image characteristics of the ^{18}F-FATPs with those of ^{13}N-NH_3 in isolated rat hearts or in a rat myocardial infarction (MI) model.

MATERIALS AND METHODS

Full details of tracer preparation and animal model are presented in the supplemental materials (available at http://jnm.snmjournals.org).

Perfused Isolated Rat Heart Study

The first-pass EF values of radiotracers were measured in isolated rat hearts perfused by the Langendorff method. Hearts were quickly excised from anesthetized rats (intraperitoneal sodium pentobarbital [0.25 mL]; Merial GmbH), placed in ice-chilled Krebs-Henseleit bicarbonate buffer (glucose at 10 mmol/L), and cannulated via the aorta (n = 8, each tracer, total rat hearts = 32). Krebs-Henseleit buffer, oxygenated with a mixture of 95% oxygen and 5% carbon dioxide, was used to perfuse the heart (flow velocities, 0.5, 4.0, 8.0, and 16.0 mL/min). The heart was stabilized for a period of 15 min, after which a bolus injection of approximately 0.925 MBq each of ^{18}F-FATP or ^{13}N-NH_3 (0.037 MBq/μL) was administered. Whole-heart radioactivity was measured over 10 min with a pair of bismuth germanate detectors interfaced to coincidence detection circuitry. Care was taken to keep the counting rate within the linear response range of the system, to prevent dead-time–induced counting rate losses during tracer injection. The total coincidence counting rate was measured as a function of time and corrected for decay. The curve was analyzed by fitting an exponentially decaying function to the data representing the tissue washout component (from 100 to 600 s). The fitted curve was extrapolated to the time of the maximum counting rate, and the value obtained was divided by the measured maximum counting rate. This ratio is a measure of the EF. As the curve was essentially linear in the fit region, possible differences between an exponential fit and a linear fit were studied. No differences were found for the determination of the EF (*5*).

Small-Animal PET Study and Image Analysis

A dedicated small-animal PET/CT scanner (Inveon; Siemens Medical Solutions) was used for in vivo imaging of the ^{18}F-FATPs and ^{13}N-NH_3. Normal (n = 3, each radiotracer) or MI (n = 3, each radiotracer) rats were anesthetized with isoflurane, placed in a cradle, and equipped with masks for anesthetic gas supply and warm water pads at the tail veins for injection. MI rats underwent imaging studies 24 h after left coronary artery occlusion (*21,22*). Dynamic small-animal PET images were acquired for 70 min after injection of 37 MBq of ^{18}F-FATP and for 30 min after injection of 37 MBq of ^{13}N-NH_3.

Acquired images were reconstructed using a 3-dimensional ordered-subset expectation maximization algorithm with 4 iterations. Reconstructed pixel sizes were 0.78 mm in the transverse and axial directions. The dimensions of the reconstructed images were 128 × 128 pixels in each of the 159 transverse slices. Data were normalized and corrected for randoms, dead time, and decay.

Analysis of the small-animal PET images was performed with PMOD software (PMOD Technologies Ltd.) (*6*). To determine pharmacokinetics, a region of interest was drawn around the heart. Time–activity curves of the ^{18}F-FATPs and ^{13}N-NH_3 were generated to obtain the counts per pixel per second. Image contrast was calculated on the basis of the Michelson contrast formula as follows (Eq. 1) (*23*):

$$\text{Image contrast}\ (\%) = \frac{\text{maximum} - \text{minimum}}{\text{maximum} + \text{minimum}} \times 100, \quad \text{Eq. 1}$$

where maximum and minimum represent the highest and lowest pixel values, respectively, in the myocardial perfusion polar map of the ^{18}F-FATPs and ^{13}N-NH_3 image.

To measure the infarction size in the small-animal PET images, reconstructed PET data were reoriented into 17 segments of polar map images. The perfusion value of each segment was measured as the average value of all pixels in the segment. The infarct area, which was defined as the fraction of the polar map segment with a perfusion value of 60% or less relative to that of the segment with the highest value, was expressed as a percentage of the left ventricular myocardium (*16*).

Statistical Analysis

Values are reported as the mean ± SD. The first-pass EF values and myocardium-to-liver and myocardium-to-lung ratios of ^{18}F-FATPs or ^{13}N-NH_3 were compared by Mann–Whitney U test. Differences in infarction size between 0–10 and 20–30 min or 0–3 and 0–6 min were compared by Wilcoxon signed-rank test. Statistical analysis was performed with SPSS software (version 21.0; IBM). P values of less than 0.05 were considered statistically significant.

RESULTS

Tracer Preparation

The chemical structures of ^{18}F-FATPs are shown in Supplemental Figure 1. The total reaction time of the ^{18}F-FATPs was within 60 min, and the overall decay-corrected radiochemical yield was approximately 15%–30%. Radiochemical purity was greater than

TABLE 1
First-Pass EF Values (%) of ^{18}F-FATPs and ^{13}N-NH_3 at Different Flow Rates

Flow rate (mL/min)	^{18}F-FPTP	^{18}F-FHTP	^{18}F-FETP	^{13}N-NH_3
0.5 (n = 2)	41.26 ± 11.51	45.30 ± 8.78	33.89 ± 10.30*	49.30 ± 4.05
4.0 (n = 2)	30.18 ± 8.90†	31.59 ± 8.73†	24.35 ± 4.38*	15.18 ± 7.29
8.0 (n = 2)	23.21 ± 6.62†	22.57 ± 6.47*	19.70 ± 3.05*	12.89 ± 6.30
16 (n = 2)	18.50 ± 4.65†	18.43 ± 3.57†	13.94 ± 1.72†	7.38 ± 3.80

*$P < 0.05$ vs. ^{13}N-NH_3 by Mann–Whitney test.
†$P < 0.01$ vs. ^{13}N-NH_3 by Mann–Whitney test.
Data are expressed as mean ± SD. EF values were measured 3 times in each isolated heart.

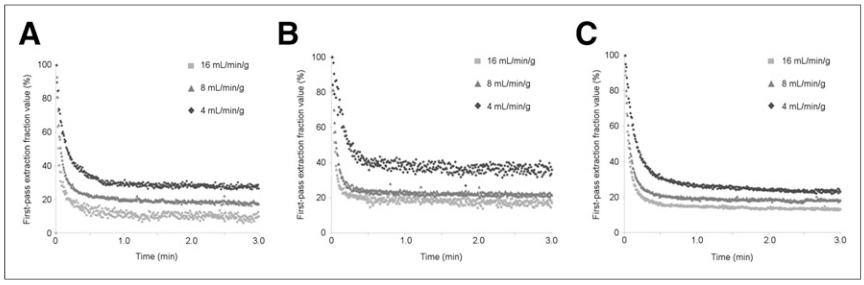

FIGURE 1. First-pass EFs as function of blood flow. Smoothed time–activity curves obtained from sequential measurements of single rat heart are shown. Flow velocities and EFs are indicated (n = 6, each flow). (A) ^{18}F-FPTP. (B) ^{18}F-FHTP. (C) ^{18}F-FETP.

98% as measured by high-performance liquid chromatography. The specific activity of ^{18}F-FATPs was greater than 6.1 TBq/μmol. The non–decay-corrected radiochemical yield of ^{13}N-NH_3 was approximately 60%–70%.

Perfused Isolated Rat Heart Study

EF values for all flow rates are shown in Table 1 and Figure 1. Lower EFs were found at higher flows, which was consistent with the ^{18}F-FATPs and ^{13}N-NH_3. The EF values of ^{18}F-FPTP, ^{18}F-FHTP, and ^{18}F-FETP were significantly higher than those of ^{13}N-NH_3 at flow rates of 4.0, 8.0, and 16 mL/min ($P < 0.05$). At the lower flow rate of 0.5 mL/min, there were no significant differences among ^{18}F-FPTP, ^{18}F-FHTP, and ^{13}N-NH_3. Only ^{18}F-FETP demonstrated a significantly lower EF value than ^{13}N-NH_3 at a flow velocity of 0.5 mL/min.

Small-Animal PET Image Characteristics

Static small-animal PET images of normal rats 10 and 30 min after intravenous injection of the ^{18}F-FATPs or ^{13}N-NH_3 are shown in Figure 2 and Supplemental Videos 1–4. The ^{18}F-FATP images demonstrated good visualization of the heart, with excellent heart-to-background contrast at each time point. High contrast between the myocardium and liver or lung was seen, whereas ^{13}N-NH_3 images showed higher liver uptake than heart uptake until 30 min after tracer injection. Time–activity curves and ratios between myocardium and liver or lung after tracer injection are shown in, respectively, Figure 2 and Tables 2 and 3. The ^{18}F-FATP time–activity curves demonstrated rapid accumulation in the myocardium (1–2 min), with stable retention for at least 60 min. The myocardium-to-liver ratios of ^{18}F-FPTP, ^{18}F-FHTP, and ^{18}F-FETP were 1.67 ± 0.21, 2.49 ± 0.08, and 2.60 ± 0.85, respectively, whereas myocardium-to-lung ratios were 3.65 ± 0.20, 5.67 ± 0.52, and 6.31 ± 0.80, respectively, 1 min after intravenous injection. These ratios increased until 30 min. By contrast, the ^{13}N-NH_3 time–activity curve revealed that the myocardium-to-liver ratio and the myocardium-to-lung ratio were 0.80 ± 0.14 and 0.93 ± 0.07, respectively, at 5 min after injection. Thereafter, liver and lung uptake of ^{13}N-NH_3 was higher than that of the myocardium. The myocardium-to-liver ratios of ^{18}F-FPTP, ^{18}F-FHTP, and ^{18}F-FETP were over 7-, 17-, and 10-fold higher, whereas myocardium-to-lung ratios were 2-, 3-, and 3-fold higher, respectively, than those of ^{13}N-NH_3 at 30 min after injection.

Representative images of MI rats acquired after acute ligation of the left coronary artery in the short-, vertical long-, and horizontal long-axes and a polar map collected 10 and 30 min after injection of ^{18}F-FATPs or ^{13}N-NH_3 are shown in Figure 3. Sharply defined myocardial defects were present with ^{18}F-FATPs or ^{13}N-NH_3 (10 min). However, defect size on the early (0–10 min) ^{13}N-NH_3

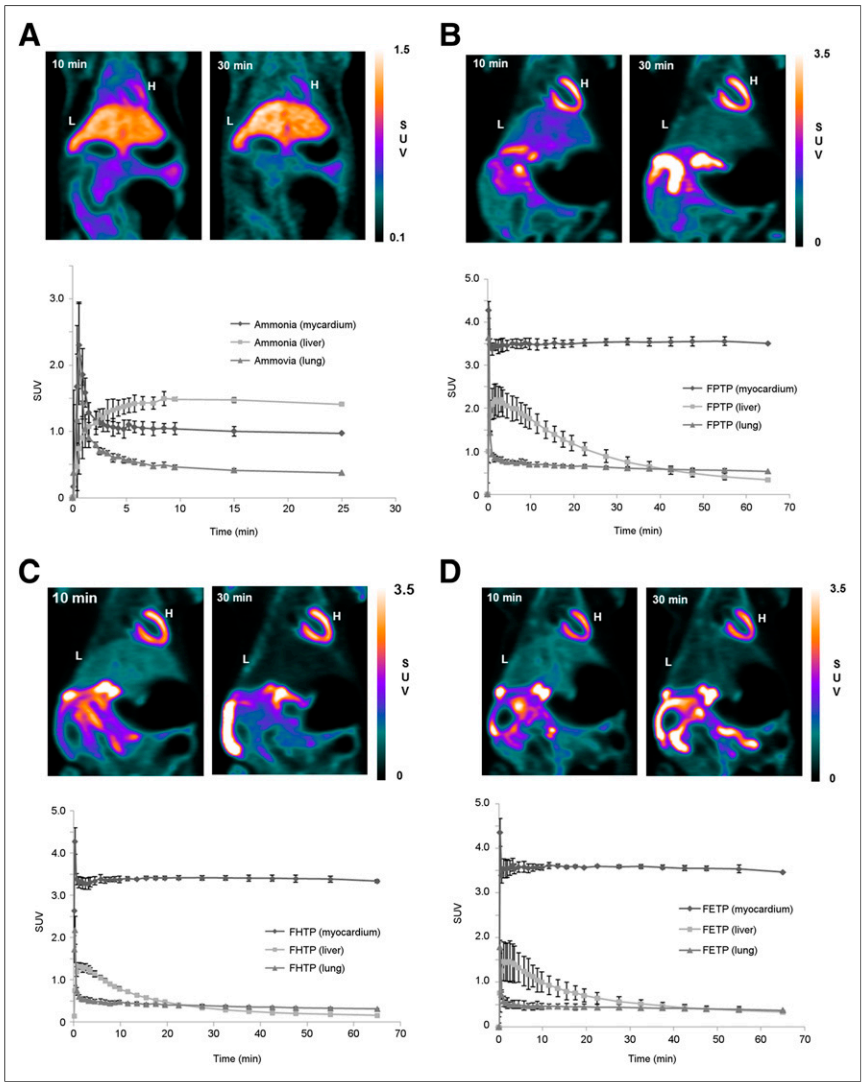

FIGURE 2. Coronal small-animal PET images and time–activity curves of normal rats after intravenous injection of 37 MBq of ^{13}N-NH_3 (A), ^{18}F-FPTP (B), ^{18}F-FHTP (C), or ^{18}F-FETP (D) (n = 3, each tracer). Heart was visible, with excellent heart-to-background contrast at each time point after ^{18}F-FATP injection. H = heart; L = liver; SUV = standardized uptake value.

TABLE 2
Myocardium-to-Liver Ratios of ^{18}F-FATPs and ^{13}N-NH_3 in Normal Rats

Tracer	Myocardium to liver				
	1 min	2 min	5 min	10 min	30 min
^{18}F-FPTP (n = 3)	1.67 ± 0.21	1.60 ± 0.22	1.74 ± 0.20*	2.10 ± 0.30*	4.87 ± 1.08*
^{18}F-FHTP (n = 3)	2.49 ± 0.08	2.60 ± 0.17*	3.05 ± 0.08*	4.36 ± 0.20*	11.9 ± 0.69*
^{18}F-FETP (n = 3)	2.60 ± 0.85	2.59 ± 0.84*	2.97 ± 0.91*	3.88 ± 1.03*	7.25 ± 1.72*
^{13}N-NH_3 (n = 3)	2.69 ± 2.35	1.12 ± 0.41	0.80 ± 0.14	0.70 ± 0.09	0.69 ± 0.04

*$P < 0.05$ vs. ^{13}N-NH_3 by Mann–Whitney test.
Data are expressed as mean ± SD (n = 3, each tracer).

images was significantly smaller than that on ^{18}F-FATPs images (0–10 min, $P = 0.027$), which might be due to spillover of radioactivity into the left ventricular or right ventricular myocardium (Supplemental Fig. 2). To confirm the spillover effect of ^{13}N-NH_3 early after intravenous injection, we compared polar map images acquired for 0–3 min and 3–6 min (Supplemental Fig. 3). The defect size and contrast ratio of ^{13}N-NH_3 images at 0–3 min were significantly lower than those at 3–6 min ($P = 0.043$), whereas ^{18}F-FATPs showed similar values for defect size and contrast ratio at 0–3 and 3–6 min (Fig. 4).

DISCUSSION

The mitochondrial membrane potential is higher in cardiomyocytes than in normal epithelial cells, and loss of mitochondrial membrane potential is an early event in cell death caused by myocardial ischemia (*24*). Similar to SPECT agents such as ^{99m}Tc-sestamibi and ^{99m}Tc-tetrofosmin, phosphonium cations accumulate in cardiomyocytes. This accumulation occurs through the higher density of mitochondria and higher electrochemical transmembrane (inside-negative) potential of cardiomyocytes, which facilitate mitochondrial uptake of phosphonium cations (*17*). Therefore, radiolabeled phosphonium cations are promising candidates for myocardial imaging (*25*).

The first radiolabeled phosphonium cation studied for use in PET was ^{11}C-triphenylmethylphosphonium (^{11}C-TPMP) (*26*). PET studies with ^{11}C-TPMP were performed to evaluate the membrane potential of heart tissue in a canine model, which was determined to be 148.1 ± 6.0 mV (inside-negative). In addition, PET studies showed that ^{11}C-TPMP accumulated in the heart immediately after intravenous injection, with a high heart-to-blood ratio (>46:1) and heart-to-lung ratio (14:1) (*27,28*). However, the use of ^{11}C-TPMP was limited because of the short half-life of ^{11}C (20 min). To provide a tracer similar to ^{11}C-TPMP but with a longer half-life, the synthesis and evaluation of ^{18}F-labeled phosphonium cations were investigated (*28*). Among them, 4-^{18}F-fluorobenzyltriphenylphosphonium (^{18}F-FBnTP) showed excellent results as a myocardial perfusion agent. ^{18}F-FBnTP was synthesized using a 4-step procedure. The 4-trimethylammoniumbenzaldehyde was used as a precursor and a third intermediate, 4-^{18}F-fluorobenzyl bromide, was reacted with triphenylphosphine to yield ^{18}F-FBnTP. ^{18}F-FBnTP was metabolically stable and demonstrated excellent characteristics as a cardiac imaging agent in healthy animals and coronary artery disease models (*11,13,18*). In a separate study, direct fluorination of tetraphenylphosphonium was investigated (*14*). Synthesis of (4-^{18}F-fluorophenyl)triphenylphosphonium (^{18}F-TPP) was performed via a direct nucleophilic substitution reaction of ^{18}F-fluoride using 4-nitrophenyltriphenylphosphonium as a precursor.

Myocardial selectivity and hepatic clearance depends on the lipophilicity and functional groups of the radiotracer. Although there is little information available with regard to the optimal lipophilicity needed for high myocardial selectivity, cationic radiotracers with log P values in the range of 0.5–1.3 are particularly useful for imaging organs with high mitochondrial density as a result of their fast membrane-penetration kinetics (*29*). Furthermore, the lipophilic interaction between the triphenylphosphonium cation and the lipid layer is attractive because the alkyl group increases lipophilicity (*30,31*). Thus, we synthesized several radiolabeled phosphonium cations and assessed lipophilicity at

TABLE 3
Myocardium-to-Lung Ratios of ^{18}F-FATPs and ^{13}N-NH_3 in Normal Rats

Tracer	Myocardium to lung				
	1 min	2 min	5 min	10 min	30 min
^{18}F-FPTP (n = 3)	3.65 ± 0.20*	4.19 ± 0.14*	4.64 ± 0.15*	5.00 ± 0.25*	5.58 ± 0.08*
^{18}F-FHTP (n = 3)	5.67 ± 0.52*	6.24 ± 0.64*	6.95 ± 0.48*	4.33 ± 0.20*	9.12 ± 0.38*
^{18}F-FETP (n = 3)	6.31 ± 0.80*	6.91 ± 1.00*	7.30 ± 1.15*	7.98 ± 1.23*	8.6 ± 1.22*
^{13}N-NH_3 (n = 3)	1.52 ± 0.07	1.53 ± 0.09	0.93 ± 0.07	2.26 ± 0.14	2.60 ± 0.05

*$P < 0.05$ vs. ^{13}N-NH_3 by Mann–Whitney test.
Data are expressed as mean ± SD (n = 3, each tracer).

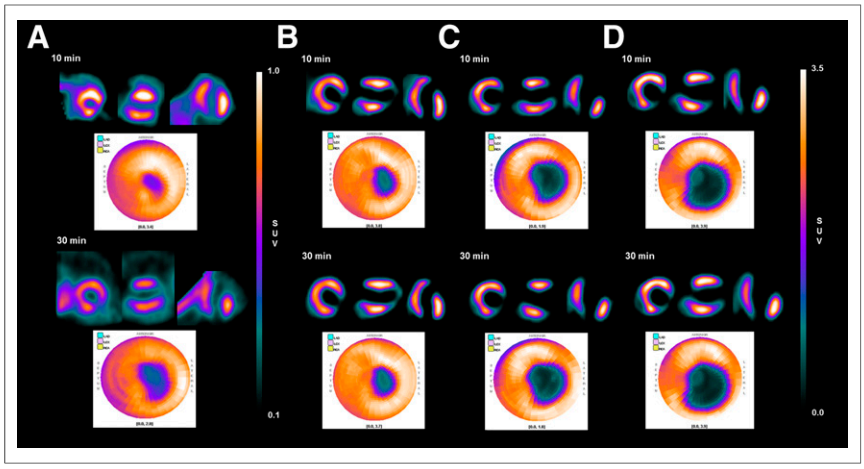

FIGURE 3. Short-, vertical long-, and horizontal long-axis and polar map images of ^{13}N-NH$_3$ (A), ^{18}F-FPTP (B), ^{18}F-FHTP (C), or ^{18}F-FETP (D) in each representative animal. Data were collected between 0–10 and 20–30 min after radiotracer injection (37 MBq). SUV = standardized uptake value.

different carbon chain lengths and with different functional groups to derive the uptake kinetics (*9,10,12,15,16*). The three ^{18}F-FATP derivatives in this study (^{18}F-FPTP, ^{18}F-FHTP, and ^{18}F-FETP) were easily synthesized from the reaction of triphenylphosphine with a precursor and exhibited appropriate cationic activity and lipophilicity for penetration of the mitochondrial membrane and accumulation within (log P = 1.31 ± 0.02, 1.78 ± 0.05, and 0.89 ± 0.02, respectively).

Measurements of first-pass EFs of ^{18}F-FATPs or ^{13}N-NH$_3$ in isolated rat hearts showed that the EF values of ^{18}F-FATPs were higher than those of ^{13}N-NH$_3$ (4.0–16.0 mL/min). Despite some limitations of the Langendorff method, including the absence of normal humoral influences and neuronal regulation, a variety of cardiovascular researchers still use this technique because it has many advantages, such as simplicity, measurement accuracy, high reproducibility, and relatively low cost (*32*). The flow rate tested in this study (0.5–16.0 mL/min) would be relevant because the expected flow rate of the Langendorff method is 7–9 mL/min for rats, and the myocardial blood flow of normal rats under isoflurane anesthesia is 4.2 ± 0.9 mL/min (*33*). Generally, flow rates in isolated rat hearts are considerably higher than those under physiologic conditions and lower EFs have been found at higher flow rates. Thus, perfusion tracers showed considerably lower values in the isolated heart model (*5*). The SPECT agent ^{99m}Tc-sestamibi demonstrated an average myocardial EF of 38% (SD = 9%) for a flow range of 0.52–3.19 mL/min/g in isolated rabbit hearts. In another study, ^{82}Rb exhibited a value of 42% (SD = 6%), which was found after injection into the femoral vein of mongrel dogs at normal resting flow rates (0.75–1.5 mL/min/g) (*34,35*). The ^{18}F-FATPs demonstrated EF values similar to ^{99m}Tc-sestamibi and ^{82}Rb. Future studies will use labeled microspheres as the gold standard in a pig model to define the relationship between ^{18}F-FATP PET flow measurements and microsphere-derived blood flow in an animal model more closely related to the human heart.

PET imaging studies of ^{18}F-FATPs in normal rats indicated rapid accumulation in the heart (1–2 min), with stable retention for at least 60 min. Hepatic clearance was fast and produced high heart-to-liver ratios. On the basis of the time–activity curve from small-animal PET images, ^{18}F-FATPs demonstrated high heart-to-liver and heart-to-lung ratios 10 min after injection. These results are consistent with high-quality myocardial images obtained with ^{18}F-FATPs. Intense liver uptake, caused by prominent hepatobiliary excretion, is frequently observed on ^{99m}Tc-based myocardial imaging (*36,37*). High liver uptake is the cause of photon scatter that may mask the detection of flow abnormalities, particularly in the inferior and inferoapical left ventricular wall (*37,38*).

The defect size and contrast ratio of ^{13}N-NH$_3$ images at 0–3 min were significantly lower than those at 3–6 min, whereas ^{18}F-FATPs showed similar values for defect size and contrast ratio at 0–3 and 3–6 min, which might be due to spillover effect of ^{13}N-NH$_3$. The spillover effect describes blurring of activity from one region of interest to another. Spillover from the left ventricle to the adjacent myocardium accounts for, on average, 10%–40% of the activity derived in the initial part of the tissue time–activity curve (*39,40*). Without spillover correction, the bidirectional cross-contamination of activities in ^{13}N-NH$_3$ PET images may affect the accuracy of the infarct size and image contrast estimates. However, the ^{18}F-FATPs showed little difference in perfusion defect size at 0–3 and 3–6 min, possibly because myocardial activity reaches a plateau within 1 min of injection.

On the basis of the EF values and parameters of the images, most measurements failed to show a statistically significant difference between ^{18}F-FATP derivatives. Furthermore, the values were obtained in an experimental study using rodent models. Further preclinical evaluation in pig models, whose hearts more closely resemble those of humans, is now under way. Further studies are needed to find the best ^{18}F-FATP derivative.

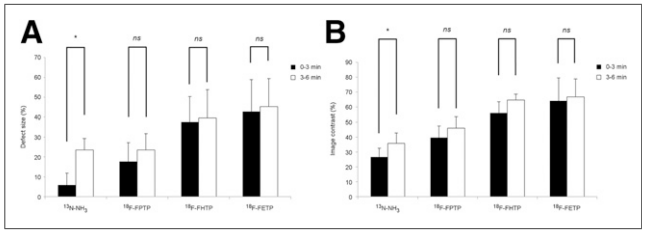

FIGURE 4. Defect size (%) (A) and image contrast (%) (B) of ^{13}N-NH$_3$, ^{18}F-FPTP, ^{18}F-FHTP, and ^{18}F-FETP between 0–3 and 3–6 min (n = 3, each tracer). *P < 0.05. ns = not significant.

CONCLUSION

The present study was performed to evaluate the imaging characteristics of ^{18}F-FATPs and compare the results with those of ^{13}N-NH$_3$. The ^{18}F-FATPs exhibited higher EF values in isolated heart, higher uptake in the myocardium, and a more rapid clearance from the liver and lung than ^{13}N-NH$_3$ in normal rats. All these characteristics enabled excellent image quality in a rat model of coronary occlusion. Moreover, ^{18}F-FATPs might accurately evaluate MI size early after tracer injection because they showed little difference in perfusion defect size at 0–3 and 3–6 min. Thus, ^{18}F-FATPs are promising ^{18}F-labeled radiopharmaceuticals for the evaluation of

myocardial perfusion by PET. The use of ^{18}F-FATP will support high-throughput clinical protocols and the widespread application of PET myocardial perfusion imaging in hospitals that do not have a cyclotron.

DISCLOSURE

The costs of publication of this article were defrayed in part by the payment of page charges. Therefore, and solely to indicate this fact, this article is hereby marked "advertisement" in accordance with 18 USC section 1734. This study was supported by a grant from the Korean Health Technology R&D Project, Ministry of Health and Welfare, Republic of Korea (HI13C0163). No other potential conflict of interest relevant to this article was reported.

ACKNOWLEDGMENT

We gratefully acknowledge the technical assistance of Hwa Youn Jang at the Department of Nuclear Medicine of Chonnam National University Hwasun Hospital.

REFERENCES

1. Small GR, Wells RG, Schindler T, Chow BJ, Ruddy TD. Advances in cardiac SPECT and PET imaging: overcoming the challenges to reduce radiation exposure and improve accuracy. *Can J Cardiol.* 2013;29:275–284.
2. Fovino LN, Saladini G, Mormino GP, Saladini F, Razzolini R, Evangelista L. Risk stratification and prognostic assessment by myocardial perfusion-gated SPECT in patients with left bundle-branch block and low-intermediate cardiac risk. *Ann Nucl Med.* 2012;26:559–570.
3. Schwaiger M, Melin J. Cardiological applications of nuclear medicine. *Lancet.* 1999;354:661–666.
4. Gibbons RJ, Valeti US, Araoz PA, Jaffe AS. The quantification of infarct size. *J Am Coll Cardiol.* 2004;44:1533–1542.
5. Huisman MC, Higuchi T, Reder S, et al. Initial characterization of an ^{18}F-labeled myocardial perfusion tracer. *J Nucl Med.* 2008;49:630–636.
6. Siegrist PT, Husmann L, Knabenhans M, et al. ^{13}N-ammonia myocardial perfusion imaging with a PET/CT scanner: impact on clinical decision making and cost-effectiveness. *Eur J Nucl Med Mol Imaging.* 2008;35:889–895.
7. Sampson UK, Dorbala S, Limaye A, Kwong R, Di Carli MF. Diagnostic accuracy of rubidium-82 myocardial perfusion imaging with hybrid positron emission tomography/computed tomography in the detection of coronary artery disease. *J Am Coll Cardiol.* 2007;49:1052–1058.
8. Yu M, Guaraldi MT, Mistry M, et al. BMS-747158-02: a novel PET myocardial perfusion imaging agent. *J Nucl Cardiol.* 2007;14:789–798.
9. Kim DY, Kim HJ, Yu KH, Min JJ. Synthesis of ^{18}F-labeled (6-fluorohexyl) triphenylphosphonium cation as a potential agent for myocardial imaging using positron emission tomography. *Bioconjug Chem.*21 2012;23:431–437.
10. Kim DY, Kim HJ, Yu KH, Min JJ. Synthesis of ^{18}F-labeled (2-(2-fluoroethoxy) ethyl)triphenylphosphonium cation as a potential agent for myocardial imaging using positron emission tomography. *Bioorg Med Chem Lett.* 2012;22:319–322.
11. Madar I, Ravert H, Nelkin B, et al. Characterization of membrane potential-dependent uptake of the novel PET tracer ^{18}F-fluorobenzyl triphenylphosphonium cation. *Eur J Nucl Med Mol Imaging.* 2007;34:2057–2065.
12. Kim D, Yu K, Bom H, Min J. Synthesis of (4-^{18}F-fluorophenyl)triphenylphosphonium as a mitochondrial voltage sensor for PET. *Nucl Med Mol Imaging.* 2007;41:561–565.
13. Madar I, Ravert HT, Du Y, et al. Characterization of uptake of the new PET imaging compound ^{18}F-fluorobenzyl triphenyl phosphonium in dog myocardium. *J Nucl Med.* 2006;47:1359–1366.
14. Cheng Z, Subbarayan M, Chen X, Gambhir SS. Synthesis of (4-^{18}F-fluorophenyl)triphenylphosphonium as a potential imaging agent for mitochondrial dysfunction. *J Labelled Comp Radiopharm.* 2005;48:131–137.
15. Kim DY, Kim HJ, Yu KH, Min JJ. Synthesis of ^{18}F-labeled (2-(2-fluoroethoxy) ethyl)tris(4-methoxyphenyl)phosphonium cation as a potential agent for positron emission tomography myocardial imaging. *Nucl Med Biol.* 2012;39:1093–1098.
16. Kim DY, Kim HS, Le UN, et al. Evaluation of a mitochondrial voltage sensor, (^{18}F-fluoropentyl)triphenylphosphonium cation, in a rat myocardial infarction model. *J Nucl Med.* 2012;53:1779–1785.
17. Min JJ, Biswal S, Deroose C, Gambhir SS. Tetraphenylphosphonium as a novel molecular probe for imaging tumors. *J Nucl Med.* 2004;45:636–643.
18. Madar I, Ravert H, Dipaula A, Du Y, Dannals RF, Becker L. Assessment of severity of coronary artery stenosis in a canine model using the PET agent ^{18}F-fluorobenzyl triphenyl phosphonium: comparison with ^{99m}Tc-tetrofosmin. *J Nucl Med.* 2007;48:1021–1030.
19. Murphy MP. Selective targeting of bioactive compounds to mitochondria. *Trends Biotechnol.* 1997;15:326–330.
20. Higuchi T, Fukushima K, Rischpler C, et al. Stable delineation of the ischemic area by the PET perfusion tracer ^{18}F-fluorobenzyl triphenyl phosphonium after transient coronary occlusion. *J Nucl Med.* 2011;52:965–969.
21. Brenner W, Aicher A, Eckey T, et al. ^{111}In-labeled CD34+ hematopoietic progenitor cells in a rat myocardial infarction model. *J Nucl Med.* 2004;45:512–518.
22. Han JH, Lim SY, Lee MS, Lee WW. Sodium ^{18}F-fluoride PET/CT in myocardial infarction. *Mol Imaging Biol.* 2015;17:214–221.
23. Freesmeyer M, Winkens T, Schierz JH. Contrast between hypervascularized liver lesions and hepatic parenchyma: early dynamic PET versus contrast-enhanced CT. *Ann Nucl Med.* 2014;28:664–668.
24. Chen LB. Mitochondrial membrane potential in living cells. *Annu Rev Cell Biol.* 1988;4:155–181.
25. Ross MF, Kelso GF, Blaikie FH, et al. Lipophilic triphenylphosphonium cations as tools in mitochondrial bioenergetics and free radical biology. *Biochemistry (Mosc).* 2005;70:222–230.
26. Fukuda H, Syrota A, Charbonneau P, et al. Use of ^{11}C-triphenylmethylphosphonium for the evaluation of membrane potential in the heart by positron-emission tomography. *Eur J Nucl Med.* 1986;11:478–483.
27. Krause BJ, Szabo Z, Becker LC, et al. Myocardial perfusion with ^{11}C-methyl triphenyl phosphonium: measurements of the extraction fraction and myocardial uptake. *J Nucl Biol Med.* 1994;38:521–526.
28. Ravert HT, Madar I, Dannals RF. Radiosynthesis of 3-^{18}F-fluoropropyl and 4-^{18}F-fluorobenzyl triarylphosphonium ions. *J Labelled Comp Radiopharm.* 2004;47:469–476.
29. Zhou Y, Liu S. ^{64}Cu-labeled phosphonium cations as PET radiotracers for tumor imaging. *Bioconjug Chem.* 2011;22:1459–1472.
30. Demura M, Kamo N, Kobatake Y. Binding of lipophilic cations to the liposomal membrane: thermodynamic analysis. *Biochim Biophys Acta.* 1987;903:303–308.
31. Ono A, Miyauchi S, Demura M, Asakura T, Kamo N. Activation energy for permeation of phosphonium cations through phospholipid bilayer membrane. *Biochemistry.* 1994;33:4312–4318.
32. Skrzypiec-Spring M, Grotthus B, Szelag A, Schulz R. Isolated heart perfusion according to Langendorff: still viable in the new millennium. *J Pharmacol Toxicol Methods.* 2007;55:113–126.
33. Croteau E, Benard F, Bentourkia M, Rousseau J, Paquette M, Lecomte R. Quantitative myocardial perfusion and coronary reserve in rats with ^{13}N-ammonia and small animal PET: impact of anesthesia and pharmacologic stress agents. *J Nucl Med.* 2004;45:1924–1930.
34. Leppo JA, Meerdink DJ. Comparison of the myocardial uptake of a technetium-labeled isonitrile analogue and thallium. *Circ Res.* 1989;65:632–639.
35. Mullani NA, Goldstein RA, Gould KL, et al. Myocardial perfusion with rubidium-82. I. Measurement of extraction fraction and flow with external detectors. *J Nucl Med.* 1983;24:898–906.
36. Nakajima K, Taki J, Shuke N, Bunko H, Takata S, Hisada K. Myocardial perfusion imaging and dynamic analysis with technetium-99m tetrofosmin. *J Nucl Med.* 1993;34:1478–1484.
37. Nuyts J, Dupont P, Van den Maegdenbergh V, Vleugels S, Suetens P, Mortelmans L. A study of the liver-heart artifact in emission tomography. *J Nucl Med.* 1995;36:133–139.
38. Kailasnath P, Sinusas AJ. Comparison of Tl-201 with Tc-99m-labeled myocardial perfusion agents: technical, physiologic, and clinical issues. *J Nucl Cardiol.* 2001;8:482–498.
39. Henze E, Huang SC, Ratib O, Hoffman E, Phelps ME, Schelbert HR. Measurements of regional tissue and blood-pool radiotracer concentrations from serial tomographic images of the heart. *J Nucl Med.* 1983;24:987–996.
40. Gambhir SS. *Quantitation of the Physical Factors Affecting the Tracer Kinetic Modeling of Cardiac Positron Emission Tomography Data* [PhD thesis]. Los Angeles, CA: University of California at Los Angeles; 1990.